

# Tailoring Quantum Chaos With Continuous Quantum Measurements

Preethi Gopalakrishnan<sup>1,\*</sup>, András Grabarits<sup>1,†</sup> and Adolfo del Campo<sup>1,2,‡</sup>

<sup>1</sup>*Department of Physics and Materials Science, University of Luxembourg, L-1511 Luxembourg, Luxembourg*  
<sup>2</sup>*Donostia International Physics Center, E-20018 San Sebastián, Spain*

We investigate the role of quantum monitoring in the dynamical manifestations of Hamiltonian quantum chaos. Specifically, we analyze the generalized spectral form factor, defined as the survival probability of a coherent Gibbs state under continuous energy measurements. We show that quantum monitoring can tailor the signatures of quantum chaos in the dynamics, such as the extension of the ramp in the spectral form factor, by varying the measurement strength and detection efficiency. In particular, a typical quantum trajectory obtained by monitoring with unit efficiency exhibits enhanced quantum chaos relative to the average dynamics and to unitary evolution without measurements.

Quantum chaos manifests itself in the spectral statistics of isolated quantum systems. In particular, chaotic systems exhibit level repulsion, which generally leads to a Wigner-Dyson distribution of nearest-level spacings, in stark contrast to the Poissonian statistics characteristic of integrable systems [1, 2]. This connection between chaos and spectral statistics has motivated the development of diagnostic tools based on the Fourier transform of energy spectra [3–7]. In this context, a prominent tool is the Spectral Form Factor (SFF), which captures correlations in the energy spectrum and exhibits a characteristic correlation hole or dip, followed by a ramp, and a plateau, in chaotic quantum systems [2, 8].

The fingerprints of quantum chaos are not limited to static spectra—they also manifest themselves in the quantum dynamics of a generic quantum superposition. While they can be appreciated in the time-evolution of quantum observables, they are often more pronounced in quantities such as the survival probability and the Loschmidt echo [6, 9–11], and closely related quantities such as the characteristic function of the work statistics [12, 13] and frame potentials [14]. Indeed, the SFF can be interpreted as the fidelity between a coherent Gibbs state and its time-evolved counterpart [15], providing a direct bridge between spectral statistics and dynamical behavior. This connection has spurred the study of SFFs on a variety of experimental platforms [16–18].

Realistic quantum systems, however, are rarely isolated, as they are generally embedded in an environment [19, 20]. This raises a natural question: how do the signatures of quantum chaos persist under open-system dynamics? Early studies revealed that classical chaos can emerge from quantum systems due to decoherence [21, 22], while other works explored how chaos influences decoherence itself [23–25].

Focusing on the spectral statistics in open systems, two complementary approaches have been developed. One generalizes the concept of spectral statistics to the generator of evolution in open quantum systems [26–30], while the other examines how the signatures of Hamiltonian quantum chaos are modified under non-unitary dynamics [15, 31–35]. Although both approaches are connected,

the latter, which we adopt here, has the advantage of focusing only on the signatures of spectral statistics that manifest themselves in quantum dynamics [36].

The signatures of quantum chaos in an isolated system are generally altered in an open setting. The interplay between chaos and decoherence can be probed via the SFF for open systems, which involves the Ulmann fidelity between an initial coherent Gibbs state and its time evolution, generally described by a mixed state [15]. Generic dephasing mechanisms have been shown to quickly suppress chaotic signatures, but when dephasing occurs on the energy eigenbasis, a smooth crossover emerges: the depth of the correlation hole decreases, and the onset of the ramp is delayed [15]. These effects are robust and persist in related tools for diagnosing quantum chaos, such as the local energy distribution in multipartite quantum systems [31].

The question arises: What kind of dynamics can enhance signatures of quantum chaos? Earlier works have shown that non-Hermitian evolution, associated with energy dephasing in the absence of quantum jumps, can amplify chaotic signatures [32, 33]. Such evolution effectively implements in the laboratory the kind of spectral filters used in computational many-body physics [7, 34, 37–39]. However, diagnosing chaos with the SFF requires long-time dynamics, up to the time associated with the onset of the plateau, set by the inverse of the average level spacing. Non-Hermitian evolution can enhance chaos, but it relies on post-selecting trajectories with no quantum jumps, whose probability decays exponentially with time, making this approach experimentally unrealistic.

Motivated by the recent experimental progress in studying the SFF [16–18], in this Letter, we investigate the fate of quantum chaos under continuous energy measurement and demonstrate that the signatures of chaos in the SFF are enhanced in a typical quantum trajectory. As a result, quantum monitoring provides a realistic, experimentally feasible route to amplify quantum chaos. Furthermore, we show that the degree of chaotic behavior exhibited in the dynamics of a quantum system can be controlled by varying the measurement strength and

efficiency.

*Evolution under continuous quantum measurements.*— The evolution of a quantum system under continuous measurements of a set of observables  $\{A_\alpha\}$  is described by the stochastic master equation (SME) [40]

$$d\rho(t) = \mathcal{L}[\rho(t)] dt + \mathcal{I}[\rho(t)] dW_t, \quad (1)$$

where the Liouvillian  $\mathcal{L}[\cdot]$  accounts for the linear open dynamics  $\mathcal{L}[\rho(t)] = -i[H, \rho(t)] - \sum_\alpha \gamma[A_\alpha, [A_\alpha, \rho(t)]]$ , and the innovation term  $\mathcal{I}[\cdot]$  describes the nonlinear stochastic backaction due to measurement:  $\mathcal{I}[\rho(t)] = \sum_\alpha \sqrt{2\gamma}(\{A_\alpha, \rho(t)\} - 2\text{Tr}[A_\alpha \rho(t)]\rho(t))$ . Here,  $dW_t$  denotes the infinitesimal increment of the Wiener process  $W_t$ , which satisfies the Itô correlation,  $\mathbb{E}[dW_t] = 0$  and  $\mathbb{E}[dW_t^2] = dt$ , such that  $\mathbb{E}[dW_t dW_s] = \delta_{t,s} dt$ . The time evolution of  $\rho(t)$  under a single realization of the measurement noise  $dW_t$  defines a quantum trajectory. Each trajectory corresponds to one possible stochastic evolution of the system conditioned on the measurement outcomes, as described by the SME in Eq. (1). Averaging over independent trajectories is equivalent to disregarding the

measurement records, since  $\mathbb{E}[dW_t] = 0$ , and yields an evolution for the ensemble-averaged state according to the standard Lindblad master equation  $d\rho(t) = \mathcal{L}[\rho(t)] dt$  [41]. We focus on monitoring a single observable, the energy of the system. Thus,  $\{A_\alpha\} = H$  and the evolution of a single trajectory is given by the SME

$$d\rho(t) = -i[H, \rho(t)] dt - \gamma[H, [H, \rho(t)]] dt + \sqrt{2\gamma}[\{H, \rho(t)\} - 2\langle H \rangle \rho(t)] dW_t. \quad (2)$$

As shown in [42], this evolution is equivalent to the dynamics that arises in the energy-driven collapse model for state reduction [43–48]. Consider a system described by the a Hamiltonian  $H$  with spectral decomposition  $H = \sum_{n=1}^d E_n |n\rangle\langle n|$ , where  $d$  is the dimension of the system Hilbert space  $\mathcal{H}$ ,  $\{E_n\}$  denote the energy eigenvalues and  $\{|n\rangle\}$  the corresponding eigenstates. As detailed in [42], for a generic initial quantum state  $\rho(0) = \sum_{nm} \rho_{nm}(0) |n\rangle\langle m|$ , its evolution under continuous energy measurements is given by

$$\rho(t) = \frac{\sum_{nm} \rho_{nm}(0) e^{-i(E_n - E_m)t - 2\gamma t(E_n^2 + E_m^2) + \sqrt{2\gamma}W_t(E_n + E_m)}}{\sum_k \rho_{kk}(0) e^{-4\gamma t E_k^2 + 2\sqrt{2\gamma}W_t E_k}} |n\rangle\langle m|. \quad (3)$$

where  $W_t$  is the stochastic integral,  $W(t) = \int_0^t dW_t$ . Note that the evolution in Eq. (3) remains pure along each trajectory, since for a given realization of  $W_t$ ,  $\rho(t)$  can be written as a normalized projector,  $\rho(t) = |\psi_t\rangle\langle\psi_t| / \langle\psi_t|\psi_t\rangle$ . Stochasticity affects only the amplitudes in  $|\psi_t\rangle$ , and purity is lost only upon averaging over many noise realizations, resulting in the mixed ensemble-averaged state described by the Lindblad equation  $d\rho(t) = -i[H, \rho(t)] dt - \gamma[H, [H, \rho(t)]] dt$ . The latter also provides an ensemble description when the quantum evolution is timed by a realistic clock subject to errors [24, 49, 50].

*Spectral Form Factor under continuous measurements.*— To probe signatures of quantum chaos under stochastic dynamics, we employ the fidelity-based definition of the spectral form factor (SFF), which remains meaningful for arbitrary quantum dynamics and is therefore directly applicable to continuous measurements. A natural generalization of the SFF to open quantum systems is given by the fidelity between the initial coherent Gibbs state,  $|\psi_\beta\rangle = \sum_n \frac{e^{-\beta E_n/2}}{\sqrt{Z(\beta)}} |n\rangle$  with  $Z(\beta) = \text{Tr}[e^{-\beta H}]$ , and its time-evolved state under stochastic dynamics. The corresponding fidelity,

$F_\beta(t, W_t) = \langle\psi_\beta|\rho(t)|\psi_\beta\rangle$ , is then given by

$$F_\beta(t, W_t) = \frac{\left| \sum_n e^{-(\beta + it - \sqrt{2\gamma}W_t)E_n} e^{-2\gamma t E_n^2} \right|^2}{Z(\beta) Z(\beta - \sqrt{8\gamma}W_t, \gamma)}, \quad (4)$$

where we define the trajectory-dependent “dephased partition function”  $Z(\beta - \sqrt{8\gamma}W_t, \gamma) = \sum_n e^{-(\beta - \sqrt{8\gamma}W_t)E_n - 4\gamma E_n^2 t}$ .

Let us next discuss the main features of the SFF under continuous monitoring. For an isolated system ( $\gamma = 0$ ), the SFF displays a characteristic dip-ramp-plateau structure [2, 51], in which the extension of the ramp, from the dip time  $t_d$  to the plateau time  $t_p$ , can be used to quantify quantum chaos [52]. Energy dephasing is known to gradually suppress the ramp in the SFF, making it shallower and delaying its onset, without affecting the plateau [15, 24]. In the context of continuous quantum measurements, this evolution arises from disregarding all measurement outcomes.

Another reference evolution corresponds to null-measurement conditioning, in which the evolution is deterministic, nonlinear, and non-Hermitian [53]. It describes quantum trajectories under the monitoring of energy with no quantum jumps and is thus restricted to short-time dynamics. Such evolution effectively filters the contribution to the SFF of each eigenvalue with a time-dependent Gaussian factor, which, for certain values

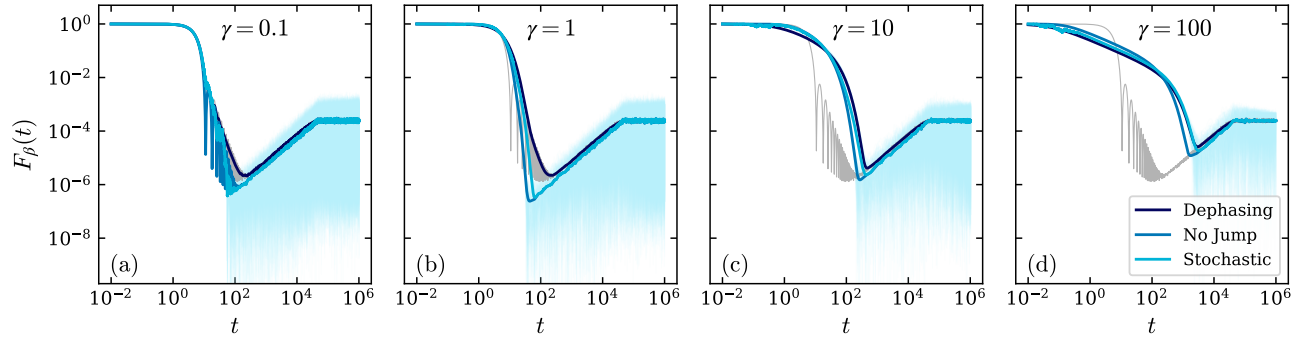


FIG. 1. Enhancement of quantum chaos under continuous monitoring in an energy-dephasing process. The time evolution of the spectral form factor (SFF) is shown for different measurement strengths  $\gamma$  in the SYK model with  $N = 26$  and  $\beta = 0$ , averaged over 250 Hamiltonian ensembles and noise realizations. The light colored lines in the background depict various individual stochastic trajectories. The SFF for unitary evolution in a closed system ( $\gamma = 0$ ) is shown by the gray curve.

of  $\gamma$ , prolongs the extension of the ramp, thus enhancing the manifestations of quantum chaos in the quantum evolution [32, 33]. The corresponding SFF can be obtained from (4) by setting  $W_t = 0$ . Jump-free trajectories are, however, rare as they are exponentially suppressed as a function of time. Their use to enhance quantum chaos is at odds with the need to probe long time scales in the SFF, given that  $t_p$  generally scales with  $d$  and thus grows exponentially with system size.

The effect of monitoring quantum chaos in the SFF, leading to (4), can be understood as supplementing the monitored dynamics under null-measurement conditioning with stochastic temporal fluctuations in the equilibrium inverse temperature. As we next illustrate, a typical trajectory under continuous energy measurements, for a suitable measurement strength, extends the ramp duration in the SFF. As such, quantum monitoring provides a natural framework to enhance the manifestations of quantum chaos probed by the SFF, without the restriction to short-time evolution intrinsic to null-measurement conditioning.

As a test bed, we consider the maximally chaotic Sachdev-Ye-Kitaev (SYK) model [54],

$$H = \sum_{1 \leq k < l < m < n \leq N} J_{klmn} \chi_k \chi_l \chi_m \chi_n, \quad (5)$$

which describes  $N$  Majorana fermions  $\{\chi_i\}$  coupled through random all-to-all quartic interactions. The couplings  $J_{klmn}$  are independently drawn from a Gaussian distribution with zero mean,  $\overline{J_{klmn}} = 0$ , and variance  $\overline{J_{klmn}^2} = 3!J^2/N^3$ , where we set  $J = 1$  for convenience. The isolated SYK model exhibits maximal quantum chaos, displaying random-matrix spectral statistics and a Lyapunov exponent that saturates the universal bound on chaos [55, 56]. Its realization has been proposed in ultracold atoms [57], digital quantum simulators [58], and disordered graphene flakes [59]. Experimental progress has been reported using NMR [60] and super-

conducting qubits [61], which provide a versatile platform for exploring the interplay between continuous measurement and many-body quantum chaos.

Figure 1 illustrates the impact of continuous monitoring on the SFF in the SYK model. We compare the SFF under stochastic evolution with two reference dynamics: (a) no-jump evolution, described by the non-Hermitian dynamics  $\frac{d}{dt}\rho = -i(H_{\text{eff}}\rho - \rho H_{\text{eff}}^\dagger) + i\text{Tr}[(H_{\text{eff}} - H_{\text{eff}}^\dagger)\rho]\rho$ , where  $H_{\text{eff}} = H - i\gamma H^2$  (b) the dissipative Lindblad evolution governed by the master equation,  $\frac{d}{dt}\rho = -i[H, \rho] - \gamma[H, [H, \rho]]$ . Note that  $F_\beta(t)$  involves a double average of the SFF, one over the Hamiltonian ensemble due to the disordered couplings  $J_{klmn}$  and the second over stochastic trajectories.

For weak measurements,  $\gamma \ll 1$ , the stochastic trajectories closely follow the evolution with no jumps as shown in Fig. 1, exhibiting the characteristic dip-ramp-plateau structure associated with chaotic dynamics. This agreement indicates that in this regime, quantum jumps are rare, and the dynamics remains effectively governed by the non-Hermitian evolution in the absence of jumps. This yields a fast decay of the SFF towards the dip, suppressing the nonuniversal part of the SFF associated with the Fourier transform of the average local energy density; see [42]. As a result, the ramp duration is prolonged as the dip time occurs earlier. By contrast, the onset of the plateau is unaffected.

Figure 1 also shows that stochastic evolution exhibits a crossover at  $\gamma \approx 1$  with increasing measurement strength  $\gamma$ . This is quantified in Fig. 2(a) by the ratio  $t_d/t_p$  of the dip and plateau times. As  $\gamma$  increases, quantum jumps become more frequent, leading to stochastic deviations from the no-jump limit. For  $\gamma \leq 1$ , the measurement-induced dynamics enhances the signatures of quantum chaos beyond the ensemble average governed by energy dephasing. Remarkably, the ramp duration is also enhanced relative to the unitary evolution shown in gray. For larger  $\gamma$ , the ramp is reduced relative to the

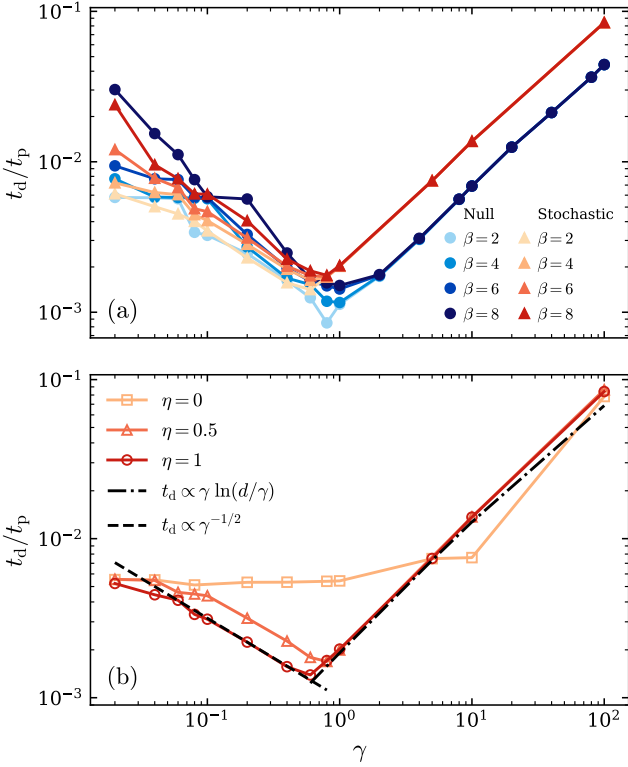


FIG. 2. (a) Tailoring quantum chaos by tuning the measurement strength. The ramp duration in the SFF is characterized by the ratio  $t_d/t_p$  of the plateau and dip times in the monitored SYK model, averaged over 250 stochastic trajectories. The ramp duration exhibits a non-monotonic behavior as a function of the measurement strength  $\gamma$ , reaching a maximum for  $\gamma_{\text{opt}} \sim \mathcal{O}(1)$ , when  $t_d/t_p$  is minimized. The dependence for small  $\gamma$  on the inverse temperature is suppressed for values  $\gamma > \gamma_{\text{opt}}$ . The limit of no jumps associated with null-measurement conditioning is shown in blue. (b) Ratio  $t_d/t_p$  as a function of the measurement strength  $\gamma$  for different values of the measurement efficiency  $\eta$ . In the absence of measurement backaction ( $\eta = 0$ ), the dip time remains nearly constant in the weak measurement regime. By contrast, for finite efficiency ( $\eta > 0$ ),  $t_d$  exhibits a pronounced nonmonotonic dependence on  $\gamma$ .

measurement-free case, and the SFF behaves similarly in the three non-Hermitian cases involving measurements, as shown in Fig. 1(c)-(d).

The enhancement of quantum chaos stems from the measurement-induced Gaussian filter  $e^{-2\gamma t E_n^2}$  at the trajectory level, with or without jumps; see Eqs. (3) and (4). This provides a physical realization of the spectral filters used in numerical analysis [7, 34, 37–39]. Monitoring enhances chaos for  $\gamma \leq 1$  by speeding up the decay of the nonuniversal part of the SFF, associated with the average density of states. It does so by suppressing high-energy contributions of the spectrum, and washes out all spectral correlations when too large ( $\gamma \geq 1$ ). Indeed, the SFF under continuous measurements follows closely that

in the no-jump limit for all values of  $\gamma$ , large and small. The case of energy dephasing leads to a Gaussian factor in the frequency domain  $e^{-\gamma t(E_n - E_m)^2}$ , rather than in the energy domain, but for large  $\gamma$ , such a filter also reduces correlations in the spectrum, suppressing chaos.

While the individual stochastic trajectories, shown as transparent lines in Fig. 1, exhibit noticeable fluctuations, their ensemble average displays a more sharply defined dip–ramp–plateau structure compared to the dissipative Lindblad dynamics. We note that the difference between the doubly averaged  $F_\beta(t, W_t)$  and the dephasing Lindblad evolution stems exclusively from the breakdown of the annealed approximation with respect to the Wiener process. This is the stochastic counterpart of the annealed approximation in disordered systems. Given two functions  $f(W_t)$  and  $g(W_t)$ , the annealed approximation involves  $\mathbb{E}[f(W_t)/g(W_t)] \approx \mathbb{E}[f(W_t)]/\mathbb{E}[g(W_t)]$ . Invoking it, the average of Eq. (4) reduces the evolution exactly to that under energy dephasing. However, as shown in [42], its breakdown is pronounced at all times, making possible the observed enhancement of quantum chaos.

*Inefficient Measurements.*— We next examine continuous measurements with finite detection efficiency  $\eta \in [0, 1]$ , which provides a natural means to tune the measurement backaction and the manifestation of quantum chaos. For any  $\eta$ , the system’s evolution is governed by the master equation,  $d\rho = -i[H, \rho]dt - \gamma[H, [H, \rho]]dt + \sqrt{2\eta\gamma}(H\rho + \rho H - 2\langle H \rangle_t\rho)dW_t$ , where  $\eta$  represents the fraction of measurement outcomes registered in the detector. This yields the SFF

$$F_\beta(t, W_t, \eta) = \frac{\sum_{n,m} e^{-\beta E_\pm^{mn}} K_t(E_n, E_m)}{Z(\beta) \sum_n e^{-\beta E_n} K_t(E_n, E_n)}, \quad (6)$$

where  $E_\pm^{mn} = E_n \pm E_m$ , and we have defined  $K_t(E_n, E_m) := \exp\left[-iE_-^{mn}t - \gamma t(E_-^{mn})^2 - \gamma\eta t(E_+^{mn})^2 + \sqrt{2\gamma\eta} E_+^{mn} W_t\right]$ . Varying  $\eta$  allows one to continuously tune the influence of measurement backaction. For  $\eta = 0$ , the dynamics reduce to purely dephasing Lindblad evolution, which minimizes quantum chaos. At full efficiency ( $\eta = 1$ ), a quantum trajectory being described by a pure state, and quantum monitoring maximally enhances chaos. This transition, shown in Fig. 2(b), highlights the role of measurement efficiency as a tunable parameter governing the onset of chaos in a continuously monitored quantum system. For finite  $\eta$  and weak dissipation, the effective filtering leads to the dip time scaling  $t_d \sim \gamma^{-1/2}$ . The crossover associated with the maximal enhancement of chaos is located for  $\eta \approx 1$ . For larger  $\gamma$ , when the evolution is governed by dephasing, the dip time scales as  $t_d \sim \gamma \ln(d/\gamma)$ , where  $d$  is the Hilbert space dimension of the Hamiltonian; see [42]. This regime reflects a Zeno-like suppression of chaos, in which strong monitoring delays the onset of universal spectral correlations.

In conclusion, we have investigated the continuous monitoring of a chaotic quantum system and identified the agency of the observer in tailoring quantum chaos. To this end, we have introduced the stochastic generalization of the SFF, given by the fidelity between a coherent Gibbs state and its time evolution under continuous quantum measurements. The amplitude of the ramp in the SFF, a manifestation of level repulsion, can be controlled by the monitoring agent by varying the strength and the efficiency of the continuous energy measurement. Remarkably, a typical quantum trajectory leads to an enhancement of quantum chaos not only with respect to the ensemble average but also when compared to the Hamiltonian unitary dynamics in the absence of measurements. Our results show how signatures of quantum chaos in the dynamics can be controlled by an external observer, and should find applications in foundations of physics and statistical mechanics [2, 62, 63], blackhole physics [51, 54], the study of complexity in quantum systems [64–66], quantum thermodynamics, and quantum simulation [16–18] and information processing [67].

*Acknowledgments.*— This project was supported by the Luxembourg National Research Fund (FNR) Grant Nos. C22/MS/17132054/AQCQNET and C24/MS/18940482/STAOpen).

*Data Availability.*— The data and source codes that support our findings are openly available [68].

---

\* preeathi.gopalakrishnan@uni.lu

† andras.grabarits@uni.lu

‡ adolfo.delcampo@uni.lu

[1] M. Mehta, *Random Matrices* (Academic Press, 1991).

[2] F. Haake, *Quantum Signatures of Chaos* (Springer, Berlin, 2010).

[3] L. Leviandier, M. Lombardi, R. Jost, and J. P. Pique, Fourier transform: A tool to measure statistical level properties in very complex spectra, *Phys. Rev. Lett.* **56**, 2449 (1986).

[4] J. Wilkie and P. Brumer, Time-dependent manifestations of quantum chaos, *Phys. Rev. Lett.* **67**, 1185 (1991).

[5] Y. Alhassid and R. D. Levine, Spectral autocorrelation function in the statistical theory of energy levels, *Phys. Rev. A* **46**, 4650 (1992).

[6] J.-Z. Ma, Correlation hole of survival probability and level statistics, *Journal of the Physical Society of Japan* **64**, 4059 (1995).

[7] R. E. Prange, The spectral form factor is not self-averaging, *Phys. Rev. Lett.* **78**, 2280 (1997).

[8] J. S. Cotler, G. Gur-Ari, M. Hanada, J. Polchinski, P. Saad, S. H. Shenker, D. Stanford, A. Streicher, and M. Tezuka, Black holes and random matrices, *J. High Energy Phys.* **2017** (5), 118.

[9] A. del Campo, J. Molina-Vilaplana, and J. Sonner, Scrambling the spectral form factor: Unitarity constraints and exact results, *Phys. Rev. D* **95**, 126008 (2017).

[10] E. J. Torres-Herrera, G. De Tomasi, M. Schiulaz, F. Pérez-Bernal, and L. F. Santos, Self-averaging in many-body quantum systems out of equilibrium: Approach to the localized phase, *Phys. Rev. B* **102**, 094310 (2020).

[11] A. K. Das, C. Cianci, D. G. A. Cabral, D. A. Zarate-Herrada, P. Pinney, S. Pilatowsky-Cameo, A. S. Matsoukas-Roubeas, V. S. Batista, A. del Campo, E. J. Torres-Herrera, and L. F. Santos, Proposal for many-body quantum chaos detection, *Phys. Rev. Res.* **7**, 013181 (2025).

[12] A. Chenu, I. L. Egusquiza, J. Molina-Vilaplana, and A. del Campo, Quantum work statistics, loschmidt echo and information scrambling, *Sci. Rep.* **8**, 12634 (2018).

[13] A. Chenu, J. Molina-Vilaplana, and A. del Campo, Work statistics, loschmidt echo and information scrambling in chaotic quantum systems, *Quantum* **3**, 127 (2019).

[14] J. Cotler, N. Hunter-Jones, J. Liu, and B. Yoshida, Chaos, complexity, and random matrices, *Journal of High Energy Physics* **2017**, 48 (2017).

[15] Z. Xu, A. Chenu, T. Prosen, and A. del Campo, Thermofield dynamics: Quantum chaos versus decoherence, *Phys. Rev. B* **103**, 064309 (2021).

[16] D. V. Vasilyev, A. Grankin, M. A. Baranov, L. M. Sieberer, and P. Zoller, Monitoring quantum simulators via quantum nondemolition couplings to atomic clock qubits, *PRX Quantum* **1**, 020302 (2020).

[17] L. K. Joshi, A. Elben, A. Vikram, B. Vermersch, V. Galitski, and P. Zoller, Probing many-body quantum chaos with quantum simulators, *Phys. Rev. X* **12**, 011018 (2022).

[18] H. Dong, P. Zhang, C. B. Dağ, Y. Gao, N. Wang, J. Deng, X. Zhang, J. Chen, S. Xu, K. Wang, Y. Wu, C. Zhang, F. Jin, X. Zhu, A. Zhang, Y. Zou, Z. Tan, Z. Cui, Z. Zhu, F. Shen, T. Li, J. Zhong, Z. Bao, H. Li, Z. Wang, Q. Guo, C. Song, F. Liu, A. Chan, L. Ying, and H. Wang, Measuring the spectral form factor in many-body chaotic and localized phases of quantum processors, *Phys. Rev. Lett.* **134**, 010402 (2025).

[19] H. P. Breuer and F. Petruccione, *The Theory of Open Quantum Systems* (Oxford University Press, 2002).

[20] W. H. Zurek, Decoherence, einselection, and the quantum origins of the classical, *Rev. Mod. Phys.* **75**, 715 (2003).

[21] Z. P. Karkuszewski, C. Jarzynski, and W. H. Zurek, Quantum chaotic environments, the butterfly effect, and decoherence, *Phys. Rev. Lett.* **89**, 170405 (2002).

[22] S. Habib, K. Jacobs, and K. Shizume, Emergence of chaos in quantum systems far from the classical limit, *Phys. Rev. Lett.* **96**, 010403 (2006).

[23] F. M. Cucchietti, D. A. R. Dalvit, J. P. Paz, and W. H. Zurek, Decoherence and the loschmidt echo, *Phys. Rev. Lett.* **91**, 210403 (2003).

[24] Z. Xu, L. P. García-Pintos, A. Chenu, and A. del Campo, Extreme decoherence and quantum chaos, *Phys. Rev. Lett.* **122**, 014103 (2019).

[25] A. del Campo and T. Takayanagi, Decoherence in Conformal Field Theory, *JHEP* **2020** (2), 170.

[26] T. Can, Random lindblad dynamics, *J. Phys. A: Math. Theor.* **52**, 485302 (2019).

[27] T. Can, V. Oganesyan, D. Orgad, and S. Gopalakrishnan, Spectral gaps and midgap states in random quantum master equations, *Phys. Rev. Lett.* **123**, 234103 (2019).

[28] L. Sá, P. Ribeiro, and T. Prosen, Complex spacing ratios: A signature of dissipative quantum chaos, *Phys. Rev. X*

**10**, 021019 (2020).

[29] L. Sá, P. Ribeiro, T. Can, and T. Prosen, Spectral transitions and universal steady states in random kraus maps and circuits, *Phys. Rev. B* **102**, 134310 (2020).

[30] L. Sá, P. Ribeiro, and T. Prosen, Integrable nonunitary open quantum circuits, *Phys. Rev. B* **103**, 115132 (2021).

[31] Z. Cao, Z. Xu, and A. del Campo, Probing quantum chaos in multipartite systems, *Phys. Rev. Res.* **4**, 033093 (2022).

[32] J. Cornelius, Z. Xu, A. Saxena, A. Chenu, and A. del Campo, Spectral filtering induced by non-hermitian evolution with balanced gain and loss: Enhancing quantum chaos, *Phys. Rev. Lett.* **128**, 190402 (2022).

[33] A. S. Matsoukas-Roubeas, F. Roccati, J. Cornelius, Z. Xu, A. Chenu, and A. del Campo, Non-hermitian hamiltonian deformations in quantum mechanics, *JHEP* **2023** (1), 60.

[34] A. S. Matsoukas-Roubeas, M. Beau, L. F. Santos, and A. del Campo, Unitarity breaking in self-averaging spectral form factors, *Phys. Rev. A* **108**, 062201 (2023).

[35] Y.-N. Zhou, T.-G. Zhou, and P. Zhang, General properties of the spectral form factor in open quantum systems, *Frontiers of Physics* **19**, 31202 (2024).

[36] A. S. Matsoukas-Roubeas, T. Prosen, and A. d. Campo, Quantum Chaos and Coherence: Random Parametric Quantum Channels, *Quantum* **8**, 1446 (2024).

[37] H. Gharibyan, M. Hanada, S. H. Shenker, and M. Tezuka, Onset of random matrix behavior in scrambling systems, *JHEP* **2018** (7), 124.

[38] I. Vallejo-Fabila, A. K. Das, D. A. Zarate-Herrada, A. S. Matsoukas-Roubeas, E. J. Torres-Herrera, and L. F. Santos, Reducing dynamical fluctuations and enforcing self-averaging by opening many-body quantum systems, *Phys. Rev. B* **110**, 075138 (2024).

[39] P. Orman, H. Gharibyan, and J. Preskill, Quantum chaos in the sparse syk model, *Journal of High Energy Physics* **2025**, 173 (2025).

[40] K. Jacobs, *Quantum Measurement Theory and its Applications* (Cambridge University Press, 2014).

[41] H. M. Wiseman and G. J. Milburn, *Quantum Measurement and Control* (Cambridge University Press, 2009).

[42] See Supplemental Material for details.

[43] N. Gisin, Quantum measurements and stochastic processes, *Phys. Rev. Lett.* **52**, 1657 (1984).

[44] G. J. Milburn, Intrinsic decoherence in quantum mechanics, *Phys. Rev. A* **44**, 5401 (1991).

[45] I. C. Percival, Primary state diffusion, *Proceedings of the Royal Society of London. Series A: Mathematical and Physical Sciences* **447**, 189 (1994).

[46] L. Diósi, N. Gisin, and W. T. Strunz, Non-markovian quantum state diffusion, *Phys. Rev. A* **58**, 1699 (1998).

[47] D. C. Brody and L. P. Hughston, Efficient simulation of quantum state reduction, *Journal of Mathematical Physics* **43**, 5254 (2002).

[48] S. L. Adler, Weisskopf-wigner decay theory for the energy-driven stochastic schrödinger equation, *Phys. Rev. D* **67**, 025007 (2003).

[49] I. L. Egusquiza, L. J. Garay, and J. M. Raya, Quantum evolution according to real clocks, *Phys. Rev. A* **59**, 3236 (1999).

[50] I. L. Egusquiza and L. J. Garay, Real clocks and the zeno effect, *Phys. Rev. A* **68**, 022104 (2003).

[51] J. S. Cotler, G. Gur-Ari, M. Hanada, J. Polchinski, P. Saad, S. H. Shenker, D. Stanford, A. Streicher, and M. Tezuka, Black holes and random matrices, *JHEP* **2017** (5), 118.

[52] J. Šuntajs, J. Bonča, T. c. v. Prosen, and L. Vidmar, Quantum chaos challenges many-body localization, *Phys. Rev. E* **102**, 062144 (2020).

[53] H. Carmichael, *Statistical Methods in Quantum Optics 2: Non-Classical Fields*, Theoretical and Mathematical Physics (Springer Berlin Heidelberg, 2009).

[54] D. Chowdhury, A. Georges, O. Parcollet, and S. Sachdev, Sachdev-ye-kitaev models and beyond: Window into non-fermi liquids, *Rev. Mod. Phys.* **94**, 035004 (2022).

[55] J. Maldacena, S. H. Shenker, and D. Stanford, A bound on chaos, *JHEP* **2016** (8), 106.

[56] N. Tsuji, T. Shitara, and M. Ueda, Bound on the exponential growth rate of out-of-time-ordered correlators, *Phys. Rev. E* **98**, 012216 (2018).

[57] I. Danshita, M. Hanada, and M. Tezuka, Creating and probing the sachdev-ye-kitaev model with ultracold gases: Towards experimental studies of quantum gravity, *Progress of Theoretical and Experimental Physics* **2017**, 083I01 (2017).

[58] L. García-Álvarez, I. L. Egusquiza, L. Lamata, A. del Campo, J. Sonner, and E. Solano, Digital quantum simulation of minimal AdS/CFT, *Phys. Rev. Lett.* **119**, 040501 (2017).

[59] M. Brzezińska, Y. Guan, O. V. Yazyev, S. Sachdev, and A. Kruchkov, Engineering syk interactions in disordered graphene flakes under realistic experimental conditions, *Phys. Rev. Lett.* **131**, 036503 (2023).

[60] Z. Luo, Y.-Z. You, J. Li, C.-M. Jian, D. Lu, C. Xu, B. Zeng, and R. Laflamme, Quantum simulation of the non-fermi-liquid state of sachdev-ye-kitaev model, *npj Quantum Information* **5**, 53 (2019).

[61] M. Asaduzzaman, R. G. Jha, and B. Sambasivam, Sachdev-ye-kitaev model on a noisy quantum computer, *Phys. Rev. D* **109**, 105002 (2024).

[62] L. D'Alessio, Y. Kafri, A. Polkovnikov, and M. Rigol, From quantum chaos and eigenstate thermalization to statistical mechanics and thermodynamics, *Advances in Physics* **65**, 239 (2016).

[63] W. H. Zurek, *Decoherence and Quantum Darwinism: From Quantum Foundations to Classical Reality* (Cambridge University Press, 2025).

[64] P. Nandy, A. S. Matsoukas-Roubeas, P. Martínez-Azcona, A. Dymarsky, and A. del Campo, Quantum dynamics in krylov space: Methods and applications, *Physics Reports* **1125-1128**, 1 (2025), quantum dynamics in Krylov space: Methods and applications.

[65] S. Baiguera, V. Balasubramanian, P. Caputa, S. Chapman, J. Haferkamp, M. P. Heller, and N. Y. Halpern, *Quantum complexity in gravity, quantum field theory, and quantum information science* (2025), arXiv:2503.10753 [hep-th].

[66] E. Rabinovici, A. Sánchez-Garrido, R. Shir, and J. Sonner, *Krylov complexity* (2025), arXiv:2507.06286 [hep-th].

[67] P. Zanardi and N. Anand, Information scrambling and chaos in open quantum systems, *Phys. Rev. A* **103**, 062214 (2021).

[68] P. Gopalakrishnan, A. Grabarits, and A. del Campo, *Data set and source codes for this article (Version v1)* (2026).

[69] B. Øksendal, *Stochastic Differential Equations* (Springer

Berlin Heidelberg, 2003).

- [70] A. S. Üstünel and M. Zakai, *Transformation of Measure on Wiener Space* (Springer Berlin Heidelberg, 2000).
- [71] Z. Palmowski and T. Rolski, A technique for exponential change of measure for markov processes, *Bernoulli* **8**, 767 (2002).

**Supplemental Material for  
“Tailoring Quantum Chaos With Continuous Quantum Measurements”**

Preethi Gopalakrishnan, András Grabarits and Adolfo del Campo

**RECALLING ITÔ CALCULUS**

In this section, we summarize the basic rules of Itô calculus used throughout this work. A Wiener process  $W_t = \int_0^t dW_s$  is composed of independent increments following Gaussian distributions with  $\mathbb{E}[dW_t] = 0$  and  $\mathbb{E}[(dW_t)^2] = dt$ . As a consequence, the Itô multiplication rules are

$$(dt)^2 = 0, \quad dt dW_t = 0, \quad (dW_t)^2 = dt. \quad (\text{S1})$$

For any stochastic process  $X_t$  governed by a stochastic differential equation,

$$dX_t = a_t dt + b_t dW_t, \quad (dX_t)^2 = b_t^2 dt, \quad (\text{S2})$$

the stochastic derivative of a function  $f(X_t, t)$ , assumed to be twice continuously differentiable, reads

$$df(X_t, t) = \frac{\partial f}{\partial t} dt + \frac{\partial f}{\partial X_t} dX_t + \frac{1}{2} \frac{\partial^2 f}{\partial X_t^2} (dX_t)^2 = \left( \frac{\partial f}{\partial t} + a \frac{\partial f}{\partial X_t} + \frac{1}{2} b^2 \frac{\partial^2 f}{\partial X_t^2} \right) dt + b \frac{\partial f}{\partial X_t} dW_t. \quad (\text{S3})$$

This is known as the Itô's formula.

As a direct consequence of Itô's formula, exponentiation of a stochastic process acquires an additional drift term. For  $dX_t = aX_t dt + gX_t dW_t$ ,

$$X_t = X_0 \exp \left[ \left( a - \frac{1}{2} g^2 \right) t + gW_t \right]. \quad (\text{S4})$$

The product of two Itô processes  $X_t$  and  $Y_t$  satisfies the Itô product rule

$$d(X_t Y_t) = X_t dY_t + Y_t dX_t + dX_t dY_t. \quad (\text{S5})$$

Similarly, the ratio  $R_t = X_t/Y_t$  satisfies

$$d\left(\frac{X_t}{Y_t}\right) = \frac{1}{Y_t} dX_t - \frac{X_t}{Y_t^2} dY_t + \frac{X_t}{Y_t^3} (dY_t)^2 - \frac{1}{Y_t^2} dX_t dY_t. \quad (\text{S6})$$

**EQUIVALENCE OF THE DYNAMICS UNDER STOCHASTIC ENERGY-DIFFUSION AND  
CONTINUOUS ENERGY MONITORING**

The energy-driven stochastic Schrödinger equation has been extensively investigated in the foundations of physics [43–46, 48], exploring quantum measurement theory and possible deviations of quantum mechanics, e.g., in the context of collapse models for state reduction. In this section, we establish its mathematical equivalence with the stochastic master equation (SME) describing continuous quantum measurements of the energy. For a pure state  $|\psi\rangle$ , the energy-driven stochastic Schrödinger equation takes the form

$$d|\psi\rangle = -iH|\psi\rangle dt - \gamma(H - \langle H \rangle)^2 |\psi\rangle dt + \sqrt{2\gamma}(H - \langle H \rangle) |\psi\rangle dW_t, \quad (\text{S7})$$

where  $\gamma$  controls the strength of the stochasticity and  $dW_t$  denotes the infinitesimal increment of the Wiener noise,  $\mathbb{E}[dW_t] = 0$ ,  $\mathbb{E}[dW_t dW_s] = \delta_{t,s} dt$ . Note that this equation is nonlinear in the quantum state as the mean energy is given by  $\langle H \rangle = \langle \psi | H | \psi \rangle$ .

Using Itô calculus, to  $\mathcal{O}(dt)$ , the equation of motion for the pure density matrix  $\rho = |\psi\rangle\langle\psi|$  is given by  $d\rho = d|\psi\rangle\langle\psi| + |\psi\rangle d\langle\psi| + d|\psi\rangle d\langle\psi|$ , which yields by direct computation

$$d\rho = -i[H, \rho] dt - \gamma \left( \{(H - \langle H \rangle)^2, \rho\} - 2(H - \langle H \rangle)\rho(H - \langle H \rangle) \right) dt + \sqrt{2\gamma}\{H - \langle H \rangle, \rho\} dW_t \quad (\text{S8})$$

$$= -i[H, \rho] dt - \gamma[H - \langle H \rangle, [H - \langle H \rangle, \rho]] dt + \sqrt{2\gamma}\{H - \langle H \rangle, \rho\} dW_t. \quad (\text{S9})$$

Simplifying the double commutator and rewriting the stochastic term, one obtains

$$d\rho = -i[H, \rho]dt - \gamma[H, [H, \rho]]dt + \sqrt{2\gamma}(\{H, \rho\} - 2\langle H \rangle \rho) dW_t, \quad (\text{S10})$$

which takes the form of the SME governing the evolution under continuous energy monitoring with unit detection efficiency, discussed in the main text. Equation (S10) corrects the expression previously quoted in the literature [e.g., Eq. (4c) in [48]].

### SOLUTION TO THE STOCHASTIC MASTER EQUATION

We consider the SME describing continuous measurement of an observable  $H$  with measurement strength  $\gamma$ ,

$$d\rho(t) = -i[H, \rho(t)]dt - \gamma[H, [H, \rho(t)]]dt + \sqrt{2\gamma}(\{H, \rho(t)\} - 2\langle H \rangle \rho(t)) dW_t, \quad (\text{S11})$$

where  $\langle H \rangle = \text{Tr}[H\rho(t)]$ . To linearize this nonlinear SME, we introduce an unnormalized density operator  $\hat{\rho}(t)$  evolving according to the linear SME

$$d\hat{\rho}(t) = -i[H, \hat{\rho}(t)]dt - \gamma[H, [H, \hat{\rho}(t)]]dt + \sqrt{2\gamma}\{H, \hat{\rho}(t)\}dW_t, \quad (\text{S12})$$

Solving Eq. (S12) in the energy eigenbasis, one finds

$$\rho(t) = \frac{\sum_{nm} \rho_{nm}(0) e^{-i(E_n - E_m)t - 2\gamma t(E_n^2 + E_m^2) + \sqrt{2\gamma}W_t(E_n + E_m)}}{\sum_k \rho_{kk}(0) e^{-4\gamma t E_k^2 + 2\sqrt{2\gamma}W_t E_k}} |n\rangle \langle m|. \quad (\text{S13})$$

Here, the Itô correction has been properly accounted for using the identity in Eq. S4. The nonlinear SME is thus mapped onto a linear stochastic evolution supplemented by a stochastic normalization factor. Applying Itô's quotient rule Eq. (S6), the evolution of the normalized state  $\rho(t) = \hat{\rho}(t)/\text{Tr}[\hat{\rho}(t)]$ , yields

$$d\rho(t) = \frac{d\hat{\rho}(t)}{\text{Tr}[\hat{\rho}(t)]} - \frac{\hat{\rho}(t) \text{Tr}[d\hat{\rho}(t)]}{\text{Tr}[\hat{\rho}(t)]^2} + \frac{\hat{\rho}(t) (\text{Tr}[d\hat{\rho}(t)])^2}{\text{Tr}[\hat{\rho}(t)]^3} - \frac{d\hat{\rho}(t) \text{Tr}[d\hat{\rho}(t)]}{\text{Tr}[\hat{\rho}(t)]^2}. \quad (\text{S14})$$

Substituting the linear SME and simplifying gives

$$d\rho(t) = -\gamma[H, [H, \rho]]dt + \sqrt{2\gamma}(\{H, \rho\} - 2\langle H \rangle \rho) dW_t - 4\gamma(\{H, \rho\} - 2\langle H \rangle \rho) \langle H \rangle dt, \quad (\text{S15})$$

where the last term arises from stochastic normalization and Itô corrections. This deterministic drift can be absorbed into a shifted Wiener increment, using the Girsanov transformation [69–71]. Specifically, defining  $d\tilde{W}_t = dW_t - 2\sqrt{2\gamma}\langle H \rangle dt$ , the drift term is canceled. The process  $\lambda_t = 2\sqrt{2\gamma}\langle H \rangle_t$  is fully determined by the noise history up to time  $t$ . Consequently, it can be considered a modified Wiener process  $\tilde{W}_t$ .

Substituting  $dW_t = d\tilde{W}_t + 2\sqrt{2\gamma}\langle H \rangle dt$  cancels the extra deterministic term, leaving the normalized nonlinear SME

$$d\rho(t) = -i[H, \rho]dt - \gamma[H, [H, \rho]]dt + \sqrt{2\gamma}(\{H, \rho\} - 2\langle H \rangle \rho) d\tilde{W}_t. \quad (\text{S16})$$

While the Wiener increment  $dW_t$  is a Gaussian random variable with probability density function  $\exp[-(dW_t)^2/(2dt)]$ , in the distribution of the shifted increment,  $d\tilde{W}_t = dW_t - \lambda_t dt$  with  $\lambda_t = \sqrt{8\gamma}\langle H \rangle_t$ , the Gaussian weight can be rewritten as

$$e^{-dW_t^2/(2dt)} = e^{-(dW_t + \sqrt{8\gamma}\langle H \rangle dt)^2/(2dt)} e^{\lambda_t^2 dt/2} e^{\lambda_t dW_t} \equiv e^{-d\tilde{W}_t^2/(2dt)} e^{\lambda_t^2 dt/2} e^{\lambda_t dW_t}. \quad (\text{S17})$$

This means each Gaussian increment can be reparameterized in terms of  $d\tilde{W}_t$  with the additional Jacobian,  $e^{\lambda_t^2 dt/2} e^{\lambda_t dW_t}$  in agreement with the Girsanov theorem. As a result, the statistical features of any arbitrary function  $f(W_t - \int_0^t ds \lambda_s)$  can always be described by the modified function  $f(\tilde{W}_t) e^{\frac{1}{2} \int_0^t ds \lambda_s^2 + \int_0^t dW_s \lambda_s}$ , where  $\tilde{W}_t$  acts as a standard Wiener noise. The products of  $e^{-d\tilde{W}_t^2/2dt} e^{\lambda_t^2 dt/2} e^{\lambda_t dW_t}$  for each  $dt$  result in  $e^{\frac{1}{2} \int_0^t ds \lambda_s^2 + \int_0^t dW_s \lambda_s}$  as the full Jacobian up to time  $t$ .

Applying this transformation to the solution of the linear SME in the energy eigenbasis, one finds that the associated Jacobian factor is independent of the individual eigenvalues. Combined with the fact that the density matrix remains normalized at all times, this implies that the Jacobian is equal to unity,

$$\text{Tr}[\rho(W_t)] = \text{Tr}[\rho(\tilde{W}_t) e^{\frac{1}{2} \int_0^t ds \lambda_s^2 + \int_0^t dW_s \lambda_s}] = e^{\frac{1}{2} \int_0^t ds \lambda_s^2 + \int_0^t dW_s \lambda_s} = 1. \quad (\text{S18})$$

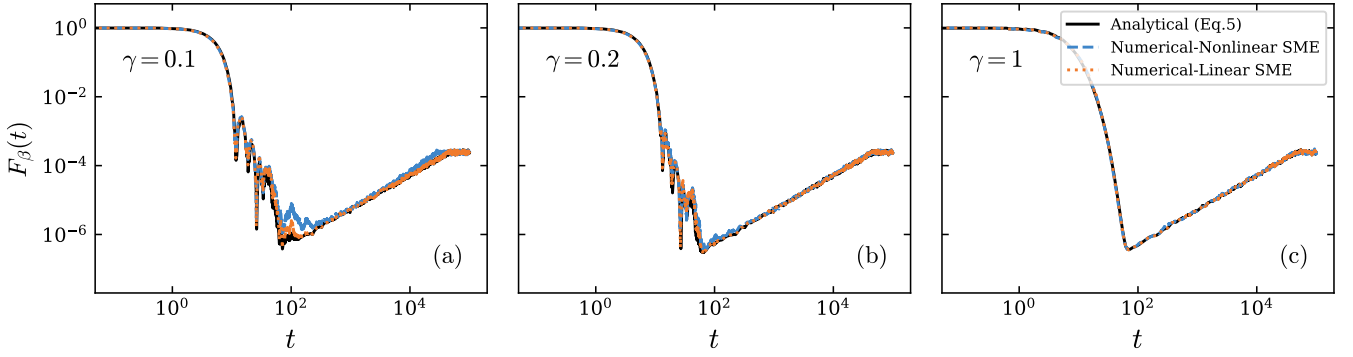


FIG. S1. Evolution of SFF for different values of  $\gamma$  in the SYK Hamiltonian with  $N = 26$ . The figure illustrates the close correspondence between numerical simulations and analytical results.

Consequently, the normalized nonlinear SME is statistically equivalent to the renormalized solution of the linear SME. In the present case, the nontrivial stochastic shift of the Wiener noise merely generates an alternative Wiener process, with observable differences arising only at the level of individual stochastic trajectories.

Figure S1 shows the evolution of the SFF for different values of the dissipation strengths  $\gamma$ . The analytical curve corresponds to Eq. (4) in the main text, which is the solution of the linear SME that was subsequently normalized. For larger  $\gamma$ , the numerical results from both linear and nonlinear SME closely follow the analytical solution, showing nearly perfect agreement. However, at lower  $\gamma$ , slight deviations in the nonlinear SSE evolution arise. Indeed, in the weak dissipation regime, the nonlinear terms –absent in the linear SME– become comparable to the leading-order drift, leading to accumulated discrepancies over time.

### STOCHASTIC EVOLUTION OF THE AVERAGE ENERGY AND ITS VARIANCE

In order to investigate the thermodynamic consequences of stochastic dephasing, we investigate the evolution of energy and its variance under continuous monitoring. These quantities provide insight into how the energy distribution of the system fluctuates in time as a consequence of the noise realization. The instantaneous average energy  $\langle H \rangle_t$  at a time  $t$  and its variance  $\langle \Delta H^2 \rangle_t$  can be expressed by means of equilibrium statistical physics, with the help of the “dephased” partition function,

$$Z(\beta - \sqrt{8\gamma}W_t, \gamma) = \sum_n e^{-(\beta - \sqrt{8\gamma}W_t)E_n - 4\gamma E_n^2 t}, \quad (\text{S19})$$

which generalizes the usual canonical partition function to include both deterministic dephasing and stochastic fluctuations.

In terms of it, the average energy and its variance can be written as derivatives of its logarithm with respect to the inverse temperature  $\beta$ .

$$\langle H \rangle_t = -\partial_\beta \log [Z(\beta - \sqrt{8\gamma}W_t, \gamma)] \quad (\text{S20})$$

$$= \frac{\sum_n E_n e^{-(\beta - \sqrt{8\gamma}W_t)E_n - 4t\gamma E_n^2}}{Z(\beta - \sqrt{8\gamma}W_t, \gamma)},$$

$$\langle \Delta H^2 \rangle_t = \partial_\beta^2 \log [Z(\beta - \sqrt{8\gamma}W_t, \gamma)]. \quad (\text{S21})$$

These stochastic quantities satisfy the differential relation

$$\begin{aligned} d\langle H \rangle_t &= \text{Tr} [H d\rho] \\ &= \sqrt{2\gamma} \text{Tr} [H (\{H, \rho_t\} - 2\langle H \rangle_t \rho_t)] dW_t \end{aligned} \quad (\text{S22})$$

$$= 2\sqrt{2\gamma} (\text{Tr} [H^2 \rho] - (\text{Tr} [H \rho])^2) dW_t$$

$$= \sqrt{8\gamma} \langle \Delta H^2 \rangle_t dW_t, \quad (\text{S23})$$

which connects fluctuations in the average energy to the instantaneous variance through the stochastic noise term. Clearly, the stochastic average  $\mathbb{E}[d\langle H \rangle_t] = 0$ . To gain further insight, one can consider the noise-average behavior of these quantities. For relatively short evolution times, the average can also be well captured by the annealed approximation, in which the averages of the numerator and denominator are taken independently over the Wiener process. Within this approximation, one finds

$$\mathbb{E}[\langle H \rangle_t] = \frac{\sum_n E_n e^{-\beta E_n}}{Z(\beta)}, \quad (\text{S24})$$

which coincides with the equilibrium Boltzmann weight average at  $t = 0$ . Thus, in the short-time or weak-dephasing limit, the stochastic dynamics preserves the equilibrium energy expectation value on average.

To see the behavior of the variance, let us introduce the conditional energy moments along a single stochastic trajectory, denoted by  $M_{k,t} := \langle H^k \rangle_t$ , and the corresponding central moments,

$$V_t := \langle \Delta H^2 \rangle_t = M_{2,t} - \mu_t^2, \quad \kappa_{3,t} := \langle (H - \mu_t)^3 \rangle_t = M_{3,t} - 3\mu_t M_{2,t} + 2\mu_t^3. \quad (\text{S25})$$

From the stochastic master equation, one obtains

$$dM_{2,t} = d\langle H^2 \rangle_t = \text{Tr}(H^2 d\rho_t) = \sqrt{8\gamma}(M_{3,t} - \mu_t M_{2,t})dW_t, \quad (\text{S26})$$

while  $d\mu_t = \sqrt{8\gamma}V_t dW_t$ . Applying Itô's rule to  $V_t$ ,

$$dV_t = dM_{2,t} - 2\mu_t d\mu_t - (d\mu_t)^2, \quad (\text{S27})$$

with  $dW_t^2 = dt$ , we get the stochastic differential equation for the closed variance,

$$dV_t = \sqrt{8\gamma}\kappa_{3,t}dW_t - 8\gamma V_t^2 dt. \quad (\text{S28})$$

The variance is influenced by the instantaneous third centered moment  $\kappa_{3,t}$ . The Itô correction leads to a strictly negative drift proportional to  $-V_t^2 dt$ , which enforces a monotonic suppression of energy fluctuations along individual trajectories. Figure S2 shows this behavior: for  $\gamma = 0$ , the unitary evolution keeps the energy distribution stable, and the variance remains constant. However, for  $\gamma > 0$ , the variance decays to zero, with increasing  $\gamma$  accelerating the collapse. While individual trajectories show strong fluctuations at intermediate times, continuous monitoring eventually localizes the state within energy eigenbasis. The decay in variance observed here is a measurement-induced effect and does not occur in unmonitored dephasing dynamics, where the variance,  $\langle \Delta H^2 \rangle_t$  remains finite.

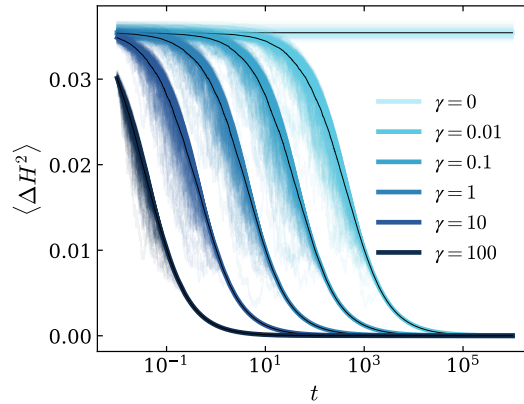


FIG. S2. Time evolution of energy variance  $\langle \Delta H^2 \rangle_t$  under continuous monitoring for different measurement strengths  $\gamma$ . The light-colored curve represents individual stochastic trajectories, while the dark black line on it indicates the trajectory-averaged behavior, which is the average of 250 trajectory realizations.

## SELF AVERAGING PROPERTY OF THE SFF

The SFF under dephasing Lindblad dynamics exhibits strong self-averaging, with individual realizations closely following the ensemble average; see Fig. S3(a). Dephasing in this setting leads to information loss, suppressing fluctuations around both the dip and plateau, so that individual trajectories show little deviation from the average [15]. Under continuous measurements, however, this self-averaging is lost as the measurement efficiency is increased. As shown in Fig. S3(b)-(c), individual stochastic trajectories fluctuate significantly, reflecting the trajectory-dependent correlations induced by measurement back-action and highlighting the inherently stochastic nature of monitored quantum chaos.

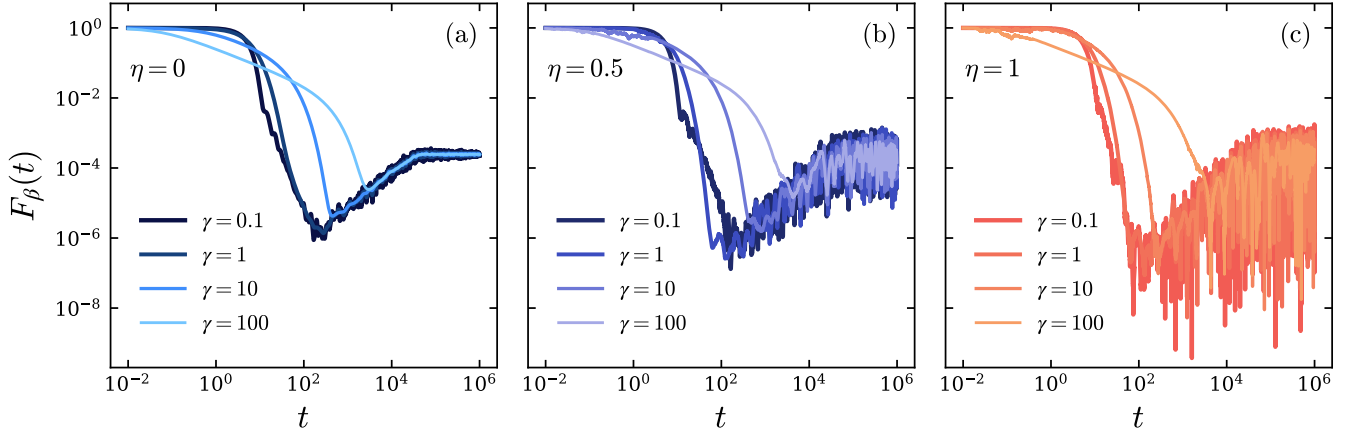


FIG. S3. Evolution of SFF for different values of the measurement strength over a single SYK Hamiltonian ( $N = 26$ ) and a single noise trajectory. The case  $\eta = 0$  is associated with the mixed-state evolution resulting from pure dephasing in the absence of the innovation term. Fluctuations in time in the SFF are then suppressed. By contrast, at the level of single trajectories under continuous quantum measurements, the amplitude of the fluctuations increases with the value of  $\eta$ . The oscillatory behavior is maximal for  $\eta = 1$  when the conditioned quantum state is pure.

## ANNEALED APPROXIMATION IN STOCHASTIC AVERAGES

Given two functions  $f(W_t)$  and  $g(W_t)$  of the Wiener noise  $W_t \sim \mathcal{N}(0, t)$ , the stochastic average of their ratio can be approximated as

$$\mathbb{E}_{W_t} \left[ \frac{f(W_t)}{g(W_t)} \right] = \frac{\mathbb{E}_{W_t} [f(W_t)]}{\mathbb{E}_{W_t} [g(W_t)]} - \frac{\text{Cov}_{W_t}[f(W_t), g(W_t)]}{\mathbb{E}_{W_t} [g(W_t)]^2} + \frac{\mathbb{E}_{W_t} [f(W_t)] \text{Var}_{W_t}[g(W_t)]}{\mathbb{E}_{W_t} [g(W_t)]^3} \dots \quad (\text{S29})$$

Thus, the annealed approximation holds whenever  $|\text{Cov}_{W_t}[f(W_t), g(W_t)]| \ll \mathbb{E}_{W_t} [g(W_t)]^2$  and  $\text{Var}_{W_t}[g(W_t)] \ll \mathbb{E}_{W_t} [g(W_t)]^2$ .

Consider the annealed approximation for the stochastic average of SFF  $F_\beta(t, W_t)$  with a fixed Hamiltonian. Provided that it holds, using the identity

$$\mathbb{E}_{W_t} [e^{\lambda W_t}] = \exp \left( \frac{\lambda^2 t}{2} \right), \quad (\text{S30})$$

the average of the numerator reads

$$\mathbb{E}_{W_t} \left[ \left| \sum_n e^{-(\beta+it-\sqrt{2\gamma}W_t)E_n} e^{-2\gamma t E_n^2} \right|^2 \right] = \mathbb{E}_{W_t} \left[ \sum_{n,m} e^{-(\beta+it)E_n} e^{-(\beta-it)E_m} e^{\sqrt{2\gamma}W_t(E_n+E_m)} e^{-2\gamma t(E_n^2+E_m^2)} \right] \quad (\text{S31})$$

$$= \sum_{n,m} e^{-(\beta+it)E_n} e^{-(\beta-it)E_m} \mathbb{E} \left[ e^{\sqrt{2\gamma}W_t(E_n+E_m)} \right] e^{-2\gamma t(E_n^2+E_m^2)} \quad (\text{S32})$$

$$= \sum_{n,m} e^{-(\beta+it)E_n} e^{-(\beta-it)E_m} e^{\gamma t(E_n+E_m)^2} e^{-2\gamma t(E_n^2+E_m^2)} \quad (\text{S33})$$

$$= \sum_{n,m} e^{-(\beta+it)E_n} e^{-(\beta-it)E_m} e^{-\gamma t(E_n-E_m)^2}. \quad (\text{S34})$$

Similarly, the stochastic average of the denominator in the expression for the SFF yields

$$\mathbb{E}_{W_t} \left[ Z(\beta)Z(\beta - \sqrt{8\gamma}W_t, \gamma) \right] = \mathbb{E}_{W_t} \left[ Z(\beta) \sum_n e^{-(\beta-\sqrt{8\gamma}W_t)E_n - 4\gamma E_n^2 t} \right] = Z(\beta)^2, \quad (\text{S35})$$

and thus, in the annealed approximation

$$\mathbb{E}_{W_t} [F_\beta(t, W_t)] \approx \frac{1}{Z(\beta)^2} \sum_{nm} e^{-\beta(E_n+E_m) - it(E_n-E_m) - \gamma t(E_n-E_m)^2}, \quad (\text{S36})$$

which is the result under energy-dephasing dynamics, i.e., when  $d\rho(t) = -i[H, \rho(t)]dt - \gamma[H, [H, \rho(t)]]dt$ . From this, it follows that the breakdown of the annealed approximation is essential in our study to quantify the measurement-induced enhancement of quantum chaos under continuous quantum measurements relative to the case of energy dephasing. Physically, it reflects the measurement backaction, which is absent in the energy dephasing case.

In the study of spectral statistics, an additional average over an ensemble of Hamiltonians  $\mathcal{E}(H)$  is also natural. This is the case in the SYK model under study due to the distribution of the couplings  $J_{klmn}$ . The study of the SFF involves then a second average  $\mathbb{E}_{\mathcal{E}(H)}[\mathbb{E}_{W_t} [F_\beta(t, W_t)]]$ . To analyze the role of the measurement backaction, we examine in Fig. S4 the difference between the annealed and quenched definitions of the SFF under stochastic averaging. We consider three distinct averaging procedures for the stochastic SFF,

$$F_\beta(t, W_t) = \frac{N(t, W_t)}{D(t, W_t)}, \quad (\text{S37})$$

expressed in terms of its numerator  $N(t, W_t)$  and denominator  $D(t, W_t)$ . The first corresponds to an annealed average over Wiener noise for a fixed Hamiltonian,

$$\frac{\mathbb{E}_{W_t} [N(t, W_t)]}{\mathbb{E}_{W_t} [D(t, W_t)]}. \quad (\text{S38})$$

The second performs annealed averages of the Wiener noise, and subsequently averages the ratio over Hamiltonian ensembles,

$$\mathbb{E}_{\mathcal{E}(H)} \left[ \frac{\mathbb{E}_{W_t} [N(t, W_t)]}{\mathbb{E}_{W_t} [D(t, W_t)]} \right]. \quad (\text{S39})$$

Lastly, we consider the double use of the annealed approximation, both with respect to the Wiener noise and the Hamiltonian disorder,

$$\frac{\mathbb{E}_{\mathcal{E}(H)}[\mathbb{E}_{W_t} [N(t, W_t)]]}{\mathbb{E}_{\mathcal{E}(H)}[\mathbb{E}_{W_t} [D(t, W_t)]]}. \quad (\text{S40})$$

In all cases, we evaluate the absolute value of relative error,  $\Delta F_\beta(W_t, t)$ , with respect to the fully quenched stochastic average,

$$\mathbb{E}_{\mathcal{E}(H)}[\mathbb{E}_{W_t} [F_\beta(t, W_t)]]. \quad (\text{S41})$$

As Fig. S4 shows, the annealed approximation is effectively broken at all relevant time scales to diagnose quantum chaos by means of the SFF. In particular, it is pronounced during the dip, ramp, and plateau regimes, as manifested by the large values of  $\Delta F_\beta(W_t, t)$  in the range of times  $10^2 - 10^4$ . The validity of the annealed approximation is restricted to short-time asymptotics when the SFF is close to unity and its early decay towards the dip.

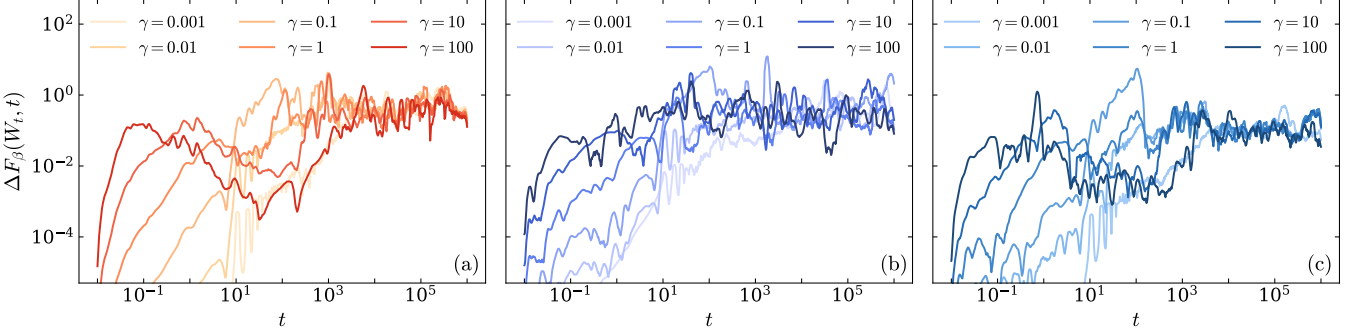


FIG. S4. Time evolution of the relative error in the annealed average for the SFF, for different values of measurement strength  $\gamma$ . The panels correspond to (a) annealed averaging over Wiener noise realizations for a fixed Hamiltonian, (b) annealed averaging over Wiener noise followed by averaging over Hamiltonian ensemble realizations, and (c) annealed averaging over both Wiener noise and Hamiltonian ensemble realizations. The curves shown are moving averages of the raw data with a window size of 100. Data are averaged over 250 stochastic trajectories.

### INEFFICIENT MEASUREMENTS AND PURITY DECAY

In the framework of continuous quantum measurements, the system undergoes a stochastic yet pure evolution, such that the density matrix  $\rho(t)$  remains pure at all times, i.e.,  $\text{Tr}[\rho^2(t)] = 1$ . This behavior is intuitive: in a perfectly efficient measurement, the measurement record contains the complete information extracted from the system, and the corresponding measurement backaction is fully correlated with this record. Consequently, the state of the system can be continuously updated based on observed measurement outcomes, yielding a single, well-defined pure-state trajectory that reflects the observer's complete knowledge of the system. The stochastic fluctuations in the measurement record merely randomize the evolution of this pure state but do not induce decoherence, as no information is lost to unmonitored channels. However, averaging many such stochastic realizations effectively disregards the individual measurement outcomes, and the state of the system becomes mixed, reproducing the decoherence expected from the corresponding unconditional master equation.

In contrast, when the measurement efficiency  $\eta < 1$ , the information acquired about the system is incomplete, and the corresponding quantum trajectories no longer remain pure. Consequently, purity decays as a function of both time and measurement efficiency  $\eta$ . The time-dependent density matrix for arbitrary  $\eta$  reads

$$\rho(t) = \frac{\sum_{nm} \rho_{nm}(0) e^{-i(E_n - E_m)t - \gamma t(E_n - E_m)^2 - \gamma \eta t(E_n + E_m)^2 + \sqrt{2\gamma\eta}W_t(E_n + E_m)}}{\sum_n \rho_{nn}(0) e^{-4\gamma\eta t E_n^2 + 2\sqrt{2\gamma\eta}W_t E_n}} |n\rangle\langle m|, \quad (\text{S42})$$

whence it follows that

$$P(t, W_t) = \text{Tr}[\rho^2(t)] = \frac{\sum_{nm} \rho_{nm}(0)^2 e^{-2\gamma t(E_n - E_m)^2 - 2\gamma \eta t(E_n + E_m)^2 + 2\sqrt{2\gamma\eta}W_t(E_n + E_m)}}{(\sum_n \rho_{nn}(0) e^{-4\gamma\eta t E_n^2 + 2\sqrt{2\gamma\eta}W_t E_n})^2}. \quad (\text{S43})$$

Alternatively, using the Hubbard-Stratonovich transformation,

$$e^{-aE^2} = \frac{1}{\sqrt{4\pi a}} \int dy e^{-\frac{y^2}{4a} - iyE}, \quad \text{Re}(a) > 0, \quad (\text{S44})$$

and the fact that for the initial coherent Gibbs state  $\rho_{nm}(0) = e^{-\beta(E_n + E_m)/2}/Z(\beta)$ , the purity in Eq. (S43) can be expressed as

$$\begin{aligned} P(t, W_t) &= \frac{\int dy \int dz e^{-\frac{z^2}{8\gamma\eta t}} e^{-\frac{y^2}{8\gamma t}} \sum_{nm} \rho_{nm}^2(0) e^{-iy(E_n - E_m)} e^{-i(z - 2i\sqrt{2\gamma\eta}W_t)(E_n + E_m)}}{\left(\int dy e^{-\frac{y^2}{16\gamma\eta t}} \sum_n \rho_{nn}(0) e^{-i(y + 2i\sqrt{2\gamma\eta}W_t)E_n}\right)^2} \\ &= \frac{\int dy \int dz e^{-\frac{z^2}{8\gamma\eta t}} e^{-\frac{z^2}{8\gamma t}} Z(\beta - 2\sqrt{2\gamma\eta}W_t + i(y + z)) Z(\beta + i(z - y))}{\left(\int dy e^{-\frac{y^2}{16\gamma\eta t}} Z(\beta + iy - 2\sqrt{2\gamma\eta}W_t)\right)^2}. \end{aligned} \quad (\text{S45})$$

These expressions explicitly capture the interplay between measurement inefficiency and dephasing, providing a quantitative description of purity decay in continuously monitored quantum systems.

It is insightful to consider the stochastic average of the purity. In the annealed approximation,

$$\mathbb{E}_{W_t}[P(t, W_t)] \approx \frac{\sum_{nm} \rho_{nm}(0)^2 e^{-2\gamma t(E_n - E_m)^2 + 2\gamma\eta t(E_n + E_m)^2}}{\sum_{nm} \rho_{nn}(0)\rho_{mm}(0)e^{-8\gamma\eta t E_n E_m}}. \quad (\text{S46})$$

By contrast, under energy dephasing, using the annealed approximation for  $\mathbb{E}[\rho(t)]$ , that reads as

$$\mathbb{E}_{W_t}[\rho(W_t, t)] \approx \sum_{nm} \rho_{nm}(0) e^{-it(E_n - E_m) - \gamma t(E_n - E_m)^2} |n\rangle\langle m|, \quad (\text{S47})$$

the purity is given by

$$P(t) = \text{Tr}[\mathbb{E}_{W_t}[\rho(W_t, t)]^2] \approx \sum_{nm} \rho_{nm}(0)^2 e^{-2\gamma t(E_n - E_m)^2}. \quad (\text{S48})$$

### SPECTRAL FORM FACTOR UNDER VARYING MEASUREMENT EFFICIENCY

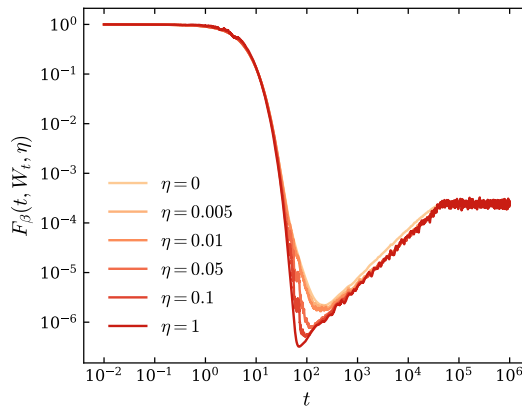


FIG. S5. Evolution of SFF under different measurement efficiency for a fixed measurement strength  $\gamma = 1$ , averaged over 250 stochastic realisations.

As depicted in Fig. S5, for all efficiencies, the SFF displays the characteristic dip–ramp–plateau structure associated with chaotic dynamics. At early times, the curves collapse, indicating that short-time dynamics is largely insensitive to the measurement efficiency. However, at intermediate times, with an increase in  $\eta$ , the dip becomes progressively deeper and sharper. The sharpening effects can be understood in terms of enhanced information extraction and higher measurement efficiency, which purify individual trajectories and strengthen spectral correlations. Enhanced quantum chaos leads to a deeper dip in the SFF and an earlier onset of the ramp, which is sharper and longer.

### STOCHASTIC SPECTRAL FORM FACTOR AND DIP TIME

To analyze the effect of continuous measurements on spectral statistics, it is useful to recall that the SFF can be decomposed into three contributions, each carrying different spectral information. Writing  $|\sum_n A_n|^2 = \sum_{n,m} A_n A_m^*$ , one finds a sum of a diagonal term with  $n = m$ , and an off-diagonal contribution with  $n \neq m$ . The latter further splits into a disconnected component without correlations among different eigenvalues and a connected component that encodes genuine two-level correlations. This decomposition reads

$$F_\beta(t, W_t) = F_\beta^{(diag)}(t, W_t) + F_\beta^{(disc)}(t, W_t) + F_\beta^{(conn)}(t, W_t), \quad (\text{S49})$$

where  $F^{(diag)}$  is time-independent and determines the contribution of self-correlation (plateau),  $F^{(disc)}$  is governed by the density of states, and  $F^{(conn)}$  reflects universal level-repulsion. The energy ensemble average of the SFF in the

annealing limit can be written as

$$\mathbb{E}_{\mathcal{E}(H)}[F_\beta(t, W_t)] = \frac{\mathbb{E}_{\mathcal{E}(H)} \left[ |\sum_n A_n(E_n, W_t)|^2 \right]}{\mathbb{E}_{\mathcal{E}(H)} \left[ Z(\beta) Z(\beta - \sqrt{8\gamma} W_t, \gamma) \right]}, \quad (\text{S50})$$

where we have defined  $A_n(E_n, W_t) = e^{-(\beta+it)E_n} e^{-2\gamma t E_n^2 + \sqrt{2\gamma} W_t E_n}$ . In terms of density of states,

$$\mathbb{E}_{\mathcal{E}(H)}[F_\beta(t, W_t)] = \frac{\iint dE dE' \mathbb{E}_{\mathcal{E}(H)}[\varrho(E, E')] A(E, W_t) A^*(E', W_t)}{\mathbb{E}_{\mathcal{E}(H)} \left[ Z(\beta) Z(\beta - \sqrt{8\gamma} W_t, \gamma) \right]} \quad (\text{S51})$$

where  $\varrho(E, E')$  is the two-point spectral density. Splitting

$$\mathbb{E}_{\mathcal{E}(H)}[\varrho(E, E')] = \mathbb{E}_{\mathcal{E}(H)}[\varrho(E)] \delta(E - E') + \mathbb{E}_{\mathcal{E}(H)}[\varrho(E) \varrho(E')] + \mathbb{E}_{\mathcal{E}(H)}[\varrho_c(E, E')], \quad (\text{S52})$$

makes the diagonal, disconnected, and connected contributions explicit.

For a large  $N$ , the DOS of SYK is given by

$$\mathbb{E}_{\text{SYK}}[\varrho(E)] = \frac{1}{2\pi} \int dt e^{-iEt} \mathbb{E}_{\text{SYK}}[e^{iHt}] \quad (\text{S53})$$

$$\simeq \sqrt{\frac{2}{\pi N}} d \exp \left( -\frac{2E^2}{N} \right). \quad (\text{S54})$$

The ensemble average of the partition function and the dephased partition function are

$$\mathbb{E}_{\text{SYK}}[Z(x)] \simeq d \exp \left( \frac{Nx^2}{8} \right), \quad (\text{S55})$$

$$\mathbb{E}_{\text{SYK}}[Z(x, \gamma)] \simeq d \left( \frac{1}{\sqrt{1+2N\gamma t}} \right) \exp \left( \frac{Nx^2}{8+16N\gamma t} \right). \quad (\text{S56})$$

The connected part of the two-point correlation function of GUE (i.e.,  $N \bmod 8 = 2$  or  $6$ ) takes the form

$$\mathbb{E}_{\text{SYK}}[\varrho_c(E, E')] \simeq - \left( \frac{\sin(2\pi r \mathbb{E}_{\text{SYK}}[\varrho(\omega)])}{\pi r} \right)^2, \quad (\text{S57})$$

with  $r = E - E'$  and  $\omega = (E + E')/2$ . The diagonal part of the SFF then reads

$$\mathbb{E}_{\text{SYK}}[F_\beta^{(\text{diag})}(t \rightarrow \infty, W_t)] = \frac{2\mathbb{E}_{\text{SYK}}[Z(2\beta - \sqrt{8\gamma} W_t, \gamma)]}{\mathbb{E}_{\text{SYK}}[Z(\beta)] \mathbb{E}_{\text{SYK}}[Z(\beta - \sqrt{8\gamma} W_t, \gamma)]} \simeq \frac{2}{d} e^{-N\beta^2/8}. \quad (\text{S58})$$

The disconnected term captures the coarse features of DOS and governs the early-time behavior of the SFF prior to the onset of correlations. Using the Gaussian form of the SYK density of states, the disconnected contribution takes the form

$$\begin{aligned} \mathbb{E}_{\text{SYK}}[F_\beta^{(\text{disc})}(t, W_t)] &= \frac{\mathbb{E}_{\text{SYK}} \left[ \left| \int dE \varrho(E) e^{-(\beta - \sqrt{8\gamma} W_t + it)E_n} e^{-2\gamma t E_n^2} \right|^2 \right]}{\mathbb{E}_{\text{SYK}}[Z(\beta)] \mathbb{E}_{\text{SYK}}[Z(\beta - \sqrt{8\gamma} W_t, \gamma)]} \\ &= \frac{\frac{1}{1+\gamma N t} \left| \exp \left[ \frac{N(\beta+it - \sqrt{8\gamma} W_t)^2}{8+8\gamma N t} \right] \right|^2}{\frac{1}{\sqrt{1+2\gamma N t}} \exp \left[ \frac{N\beta^2}{8} \right] \exp \left[ \frac{N(\beta - \sqrt{8\gamma} W_t)^2}{8+16N\gamma t} \right]}, \end{aligned} \quad (\text{S59})$$

while the connected part is given by

$$\mathbb{E}_{\text{SYK}}[F_\beta^{(\text{conn})}(t, W_t)] = - \frac{\int_{-\infty}^{\infty} d\omega \int_{-\infty}^{\infty} dr \left( \frac{\sin(2\pi r \mathbb{E}_{\text{SYK}}[\varrho(\omega)])}{\pi r} \right)^2 \exp \left[ -2\beta\omega - itr - \gamma tr^2 - 4\gamma t\omega^2 + 2\sqrt{2\gamma} W_t \omega \right]}{\mathbb{E}_{\text{SYK}}[Z(\beta)] \mathbb{E}_{\text{SYK}}[Z(\beta - \sqrt{8\gamma} W_t, \gamma)]}. \quad (\text{S60})$$

The integral over the relative coordinate  $r$  can be evaluated in a closed form. In the strong dissipation regime ( $\gamma \gg 1$ ), for late times  $t \gg d/\sqrt{N}$ , where the Gaussian suppresses all but the narrow support of the sinc kernel, one obtains

$$\int_{-\infty}^{\infty} dr \left( \frac{\sin(k(\omega)r)}{\pi r} \right)^2 e^{-itr - \gamma tr^2} \approx \frac{k(\omega)}{\pi}, \quad (\text{S61})$$

with  $k(\omega) = 2\pi \mathbb{E}_{\text{SYK}}[\varrho(\omega)] = 2\pi \sqrt{\frac{2}{\pi N}} d e^{-\frac{2\omega^2}{N}}$ . Carrying out the remaining  $\omega$ -integral and normalizing by the dephased partition function yields, at leading order in  $t$ ,

$$\mathbb{E}_{\text{SYK}}[F_{\beta}^{(conn)}(t, W_t)] \simeq \frac{1}{2d^2} \sqrt{\frac{N}{8\pi}} t \exp \left[ \frac{\beta^2}{4t\gamma} - \frac{\beta W_t}{\sqrt{2t\gamma}} + \frac{W_t^2}{4N\gamma t^2} - \frac{N\beta^2}{8} \right]. \quad (\text{S62})$$

The dip time  $t_d$  is determined by crossing the disconnected and connected pieces. Using  $F_{\beta}^{(disc)}(t, W_t = 0) = F_{\beta}^{(conn)}(t, W_t = 0)$  at  $\beta = 0$ , we get the dip time,

$$t_d(\gamma) = 6\gamma W \left( \frac{1}{6\gamma} \left( \frac{8d^2\sqrt{2\pi}}{n\sqrt{\gamma}} \right)^{2/3} \right), \quad (\text{S63})$$

where  $W(x)$  is the Lambert function.

Note that Eqs. (S58), (S59) and (S62) hold only for small  $\beta$ . However, they can be used for estimating the SFF for finite  $\beta$  as well.